Inorganic Chemistry

Article

pubs.acs.org/IC

Crystal and Magnetic Structure in Co-Substituted $BiFeO_3$

Izabela Sosnowska,*[,†] Masaki Azuma,[‡,§] Radosław Przeniosło,[†] Dariusz Wardecki,[†] Wei-tin Chen,[§,#] Kengo Oka,[‡,§] and Yuichi Shimakawa[§]

[†]Institute of Experimental Physics, Physics Faculty, University of Warsaw, Hoża 69, 00-681 Warsaw, Poland

[‡]Materials and Structures Laboratory, Tokyo Institute of Technology, 4259 Nagatsuta, Midori-ku, Yokohama, Kanagawa 226-8503, Japan

[§]Institute for Chemical Research, Kyoto University, Uji, Kyoto, 611-0011, Japan

Supporting Information

ABSTRACT: Ultra-high-resolution neutron diffraction studies of $BiFe_{0.8}Co_{0.2}O_3$ show a transition from a cycloidal space modulated spin structure at T = 10 K to a collinear G-type antiferromagnetic structure at T = 120 K. The model of antiparallel directions of Fe^{3+} and Co^{3+} magnetic moments at the shared Wyckoff position describes well the observed neutron diffraction intensities. On heating above RT, the crystal structure of $BiFe_{0.8}Co_{0.2}O_3$ changes from a rhombohedral $R3c$ to a monoclinic Cm. At 573 K only the Cm phase is present. The collinear C-type antiferromagnetic structure is present in the Cm phase of $BiFe_{0.8}Co_{0.2}O_3$ at RT after annealing.

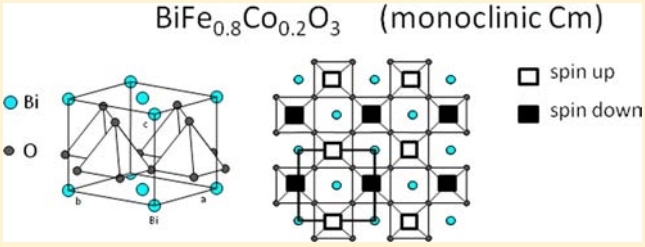

1. INTRODUCTION

Multiferroics (see, for example, refs 1−5) are promising materials for the design and synthesis of multifunctional materials. They are important for their unique and strong coupling of electric, magnetic, and structural order parameters, giving rise to simultaneous ferroelectricity, ferromagnetism, and ferroelasticity (see, for example, ref 1). Multiferroics maintain a magnetization and dielectric polarization, which can be modified by an electric field and magnetic field, respectively.[5] For this reason, multiferroic materials are being considered for potential applications as magnetic recording media, information storage devices, and sensors.[2,6,7]

Bismuth ferrite ($BiFeO_3$) has been a focal point of research because its bulk form is an antiferromagnetic, ferroelectric, and ferroelastic multiferroic material with the ferroelectric Curie temperature T_C = 1103 K and antiferromagnetic Néel temperature T_N = 643 K,[1] i.e., much above RT. The crystal structure of $BiFeO_3$ is described with the rhombohedral space group $R3c$.[8,9] Recent modifications to monoclinic Cc[10] or even triclinic $P1$[11] $BiFeO_3$ crystal structures were found. The combined action of exchange and spin−orbit interactions produces in $BiFeO_3$ a magnetic structure different from a perfect antiferromagnetic ordering. $BiFeO_3$ shows a space-modulated spiral structure (SMSS) superimposed on the antiferromagnetic G-type ordering. The period of this SMSS order is 62 nm,[12,13] and its studies require ultra-high-resolution neutron diffraction. Recent SANS studies show a small ferromagnetic component[14] that rotates, in a way similar to the SMSS ordering, i.e., producing a helimagnetic ordering with vanishing magnetization in the bulk.[14]

The SMSS ordering in $BiFeO_3$ is stable, and it persists when the temperature varies from 4 K to the Néel temperature (see, for example, refs 15 and 16). For practical application of $BiFeO_3$ it is important to have a multiferroic material possessing the magnetoelectric (ME) effect at room temperature. It was noticed that in pure $BiFeO_3$ only a quadratic magnetoelectric effect appears,[17,18] whereas when part of the Bi atoms are replaced by La, a linear magnetoelectric effect can be observed.[18] The modification of the spin structure is therefore the key issue for the realization of $BiFeO_3$-based ferromagnetic ferroelectrics. The improvement of the magnetic behavior of $BiFeO_3$ can be obtained via some suitable substitution at Bi or Fe sites (see, for example, ref 18) or by changing the sample dimensionality to a thin-layer material[19] or to nanoscale crystallites (for example, refs 20 and 21).

Many attempts to add ferromagnetic properties to the $BiFeO_3$ compound by both A and B site substitutions (see, for example, refs 22−29) were made. Neutron diffraction studies on $Bi_{1-x}La_xFeO_3$ and $BiFe_{1-y}Mn_yO_3$ show that the SMSS modulation period in $BiFeO_3$ grows with La (Bi, A-substitution)[26] and Mn (Fe, B-substitution).[27] The SMSS magnetic structure in these doped $BiFeO_3$ materials remains. The effectiveness of the substitution process in $BiFeO_3$ can be directly observed by using ultra-high-resolution neutron diffraction.[26,27] This methodology is applied also in the present study of cobalt doping in $BiFeO_3$.

The influence of Co substitution for Fe in high-quality polycrystalline samples prepared by high-pressure synthesis was investigated using synchrotron (SR) and X-ray diffraction.[28,29] It was shown that the crystal structure of $BiFe_{1-x}Co_xO_3$ changed from $R3c$ to tetragonal $P4mm$ with $x > 0.4$. Later, it

Received: September 25, 2013
Published: November 1, 2013

   dx.doi.org/10.1021/ic402427q | Inorg. Chem. 2013, 52, 13269−13277

was reported by the same authors that a monoclinic phase with symmetry *Cm* appears for $x \approx 0.3$.[29] The rotation of electric polarization was found to depend on the composition and temperature. The X-ray diffraction studies for concentration $x = 0.2$ reveal the tetragonal phase (*P*4*mm*) at RT and rhombohedral (*R*3*c*) above RT.[28] The transition from a tetragonal to a rhombohedral structure was also predicted by a first-principles calculations.[30]

The structure of $BiFe_{0.5}Co_{0.5}O_3$ ceramics was investigated[31] by using X-ray diffraction. The authors claim that $BiFe_{0.5}Co_{0.5}O_3$ has a structural transformation from a rhombohedral (space group *R*3c) to a cubic structure (space group *I*23). This new result[31] has not been confirmed by other authors.

Recently, the magnetic moment of Co^{3+}, $\mu_{Co3+} = 2.82\ \mu_B$, was determined in $BiFe_{1-x}Co_xO_3$ for $x = 0.01$ and 0.02 at RT.[24] It was suggested that the state of Co^{3+} has been changed from a low-spin (LS) state below 150 K to an intermediate-spin state (IS) above 150 K.[24] The cycloidal spiral SMSS model[12] was used in the interpretation of the magnetic structure for both $x = 0.01$ and 0.02 compositions.[25] The magnetic properties of $BiFe_{1-x}Co_xO_3$ with low concentration of Co ($x < 0.05$) were studied by various groups, and it was suggested that Co doping greatly influences the bulk magnetic properties of $BiFeO_3$, producing a ferromagnetic net moment.[22,23] An improvement of the dielectric constant and ferromagnetic properties of Co-doped $BiFeO_3$ nanotubes[32] and the application of Co-substituted $BiFeO_3$ in sorption removal of dye molecules from aqueous solution were reported recently.[33]

The influence of Co doping on the crystal structure of $BiFeO_3$ and possible change of the SMSS magnetic structure of $BiFe_{1-x}Co_xO_3$ ($x = 0.2$) are the subject of present ultra-high-resolution neutron diffraction studies.

2. EXPERIMENTAL SECTION

A polycrystalline ceramic sample of $BiFe_{0.8}Co_{0.2}O_3$ was prepared at Kyoto University by high-pressure synthesis at 4 GPa. The $BiFe_{0.8}Co_{0.2}O_3$ sample was prepared from Bi_2O_3, Co_3O_4, and Fe_2O_3. The stoichiometric mixtures were charged in gold capsules of 3.6 mm diameter and 5 mm height and were compressed to 4 to 6 GPa, followed by heat treatment at 1000 °C for 30 min in a cubic anvil type high-pressure apparatus. A 10 mg amount of the oxidizing agent $KClO_4$ was added to the top and bottom of the capsule in a separate manner. The obtained sample was crushed and washed with distilled water to remove the remaining KCl. The as-prepared sample contained only the rhombohedral phase described with the space group *R*3*c*. The X-ray diffraction patterns were collected with Cu Kα radiation. The as-prepared sample does not show impurity phases. Part of the $BiFe_{0.8}Co_{0.2}O_3$ sample was annealed at 573 K and cooled to RT. This sample will be referred to as "annealed".

Neutron diffraction studies of $BiFe_{0.8}Co_{0.2}O_3$ and $BiFeO_3$ (reference polycrystalline sample[34]) have been performed by using the time-of-flight (TOF) neutron diffractometer HRPD at the ISIS facility.[35] HRPD can achieve a resolution of $\Delta d/d = 4 \times 10^{-4}$. Diffraction data were collected with the sample in a flat vanadium container of 15 × 20 mm surface area and 5 mm thickness, placed inside the closed cycle cooler and later inside a furnace. Data were recorded at several temperatures between 10 and 573 K. The measurements were done for the interplanar *d*-spacing range of 4.3−4.7 Å using the backscattering geometry (TOF range 200−240 ms), i.e., in the region with the most intense magnetic satellites around the (101) and (003) positions (hexagonal setting of the space group *R*3*c*). The measurements were also performed for the interplanar *d*-spacing range of 0.65−2.5 Å using the backscattering geometry (TOF range 30−130 ms) in order to determine the parameters of the crystal structure. For some measurements, the 90° scattering bank was also used ($0.84 < d < 3.90$ Å). The measured neutron diffraction intensities have been normalized and corrected for detector efficiency effects using previously recorded vanadium calibration data. All standard parameters of the crystal structure are determined as a function of temperature by using the FULLPROF program.[36]

3. RESULTS

Backscattering neutron diffraction studies of the $BiFe_{0.8}Co_{0.2}O_3$ magnetic ordering require neutrons, of about 9 Å wavelength. Neutron flux at this wavelength is quite low, and the intensity of scattered neutrons was not sufficient to justify a reliable line shape analysis. The analysis of the sample microstructure is generally difficult in TOF diffractometers because of the complex line shape. Therefore our studies are focused on the analysis of the average crystal and magnetic structure rather than on the sample microstructure.

In the temperature range 10−195 K, we observe one magnetic phase transition, while in the temperature range 295−573 K, we observe one structural and one magnetic phase transition. All new phases were identified, and their parameters were refined.[36] Details of the structure analysis are presented in Sections 3A (low-temperature studies), 3B (high-temperature studies), and 3C (annealed sample studies).

3A. Neutron Diffraction Studies of $BiFe_{0.8}Co_{0.2}O_3$ below RT. The neutron powder diffraction patterns of $BiFe_{0.8}Co_{0.2}O_3$ observed between 10 K and RT show a single-phase crystal structure described by using the widely known $BiFeO_3$-type rhombohedral crystal structure (space group *R*3*c*) (see, for example, refs 9 and 37). Due to the resolution of the instrument and due to possible sample morphology contributions (grain size and microstrains), it is not possible to observe subtle distortions of the rhombohedral structure that were described for the parent $BiFeO_3$ material with the monoclinic *Cc*[10] or triclinic *P*1[11] space groups.

The effect of Co substitution on the $BiFeO_3$ structure can be examined using structural parameters obtained for $BiFeO_3$ and $BiFe_{0.8}Co_{0.2}O_3$; see Table 1.

For $BiFe_{0.8}Co_{0.2}O_3$ and $BiFeO_3$ (with similar SMSS ordering) at 10 K, the lattice parameter ratio c/a equals 2.475 and 2.483, respectively; that is, the former is less distorted than the pure $BiFeO_3$ from the ideal cubic perovskite aristotype, for which $c/a = \sqrt{6} \approx 2.449$. A model of the hexagonal unit cell of the $BiFeO_3$ crystal structure described with the space group *R*3*c* is shown in Figure 1.

The atomic displacement factors for Bi ions are large when compared with those for Fe/Co ions. This effect was observed in earlier studies, e.g., in refs 8 and 9. This effect may be related with either anomalous thermal vibrations of Bi ions or contributions from static disorder to the atomic displacement factors for Bi ions. Such an effect was earlier observed in perovskites. The refined ordered magnetic moment for the shared Fe/Co positions in $BiFe_{0.8}Co_{0.2}O_3$ is considerably smaller than that of Fe ions in $BiFeO_3$.

The values of the bond lengths and bond angles for $BiFeO_3$ and $BiFe_{0.8}Co_{0.2}O_3$ observed at $T = 10$ K and $T = 295$ K (calculated from the data given in Table 1) are presented in Table 2.

The Fe/Co−O bond length dispersion, Δ_6, is calculated for all bond lengths in the Fe/Co−O_6 octahedra by using the formula

$$\Delta_N = \frac{1}{N}\sum_{j=1}^{N}\left(\frac{dMO_j - \langle dMO\rangle}{\langle dMO\rangle}\right)^2 \quad (1)$$

dx.doi.org/10.1021/ic402427q | Inorg. Chem. 2013, 52, 13269−13277

Table 1. Parameters of the Rhombohedral Crystal Structure of $BiFeO_3$ and $BiFe_{0.8}Co_{0.2}O_3$ Determined by Neutron Diffraction at 10 and 295 K[a]

	1	2	3	4
sample	$BiFeO_3$ (x = 0) T = 10 K	BFCO (x = 0.20) T = 10 K	$BiFeO_3$ (x = 0) T = 295 K	BFCO (x = 0.20) T = 295 K
$a = b$ [Å]	5.57174(1)	5.54216(2)	5.57973(1)	5.55507(1)
c [Å]	13.83512(2)	13.71829(2)	13.87208(4)	13.77001(4)
c/a	2.48309(1)	2.47526(1)	2.48615(1)	2.47882(1)
z(Fe/Co)	0.2205(1)	0.2229(1)	0.2208(1)	0.2230(1)
x(O)	0.4458(1)	0.4471(1)	0.4460(1)	0.4471(1)
y(O)	0.0186(1)	0.0170(1)	0.0174(2)	0.0170(1)
z(O)	0.9516(1)	0.9550(1)	0.9517(1)	0.9550(1)
B(Bi) [Å^2]	0.089(23)	0.193(13)	0.430(26)	0.570(14)
B(Fe/Co) [Å^2]	0.129(22)	0.071(13)	0.109(26)	0.420(14)
B(O) [Å^2]	0.262(21)	0.248(8)	0.388(25)	0.690(10)
δ	0.0046(1)	0.0044(1)	0.0045(1)	--
M[μ_B]	4.28(2)	3.33(3)	3.98(2)	3.12(3)
R_p [%]	4.80	4.68	4.36	4.78
R_{wp} [%]	5.34	5.52	4.92	5.35
R_{exp} [%]	4.75	3.57	4.46	4.95
R_{Bragg} [%]	3.39	6.04	4.43	5.18
R_{mag} [%]	3.86	12.7	5.79	3.17
χ^2	1.26	2.38	1.22	1.17

[a]The modulated magnetic ordering model is taken from refs 12 and 34 with the modulation vector (δ,δ,0) and the ordered magnetic moment M. The $BiFe_{0.8}Co_{0.2}O_3$ at 295 K has a G-type AFM ordering. The agreement factors are given.

where N is the number of bonds in the polyhedron (N = 6 for octahedra). In the next sections for pyramidal coordinations, N = 5 will also be used. The value of ⟨dMO⟩ is the mean Fe/Co−O bond length in the Fe/Co−O polyhedron. The displacement of the Bi ions along the c-axis with respect to the nearest O ions is denoted as s in the notation of Megaw and Darlington.[37] The displacement of the Fe/Co ions along the c-axis with respect to the center of the Fe/CoO_6 octahedra is denoted as t in the notation of Megaw and Darlington.[37] The values of these displacements can be calculated by using the atomic coordinates given in Table 1 as discussed in refs 37 and :

$$s = 1 - z_O \quad (2)$$

$$t = z_{Fe} - z_O + \frac{3}{4} \quad (3)$$

Although it is known that the electric polarization of $BiFeO_3$ is considerably larger than that calculated assuming simple displacements of point charges along the polar axis (c-axis), it is important to compare the Bi and Fe/Co displacements in $BiFe_{0.8}Co_{0.2}O_3$ and $BiFeO_3$. In Table 2, one can see that both the Bi (s) and Fe/Co (t) displacements are smaller for $BiFe_{0.8}Co_{0.2}O_3$ when compared to $BiFeO_3$. There is no temperature change (within statistical errors) of the displacement parameters s and t for $BiFe_{0.8}Co_{0.2}O_3$, while for $BiFeO_3$ a weak temperature dependence can be seen.

The FeO_6 octahedra in both $BiFeO_3$ and $BiFe_{0.8}Co_{0.2}O_3$ are strongly distorted: the O^{2-} ions form two regular triangles, both perpendicular to the c-axis, one above and one below the Fe/Co ions. There are three (equal) shorter Fe/Co−O distances for the upper triangle and three (equal) longer Fe/Co−O distances for the lower triangle.

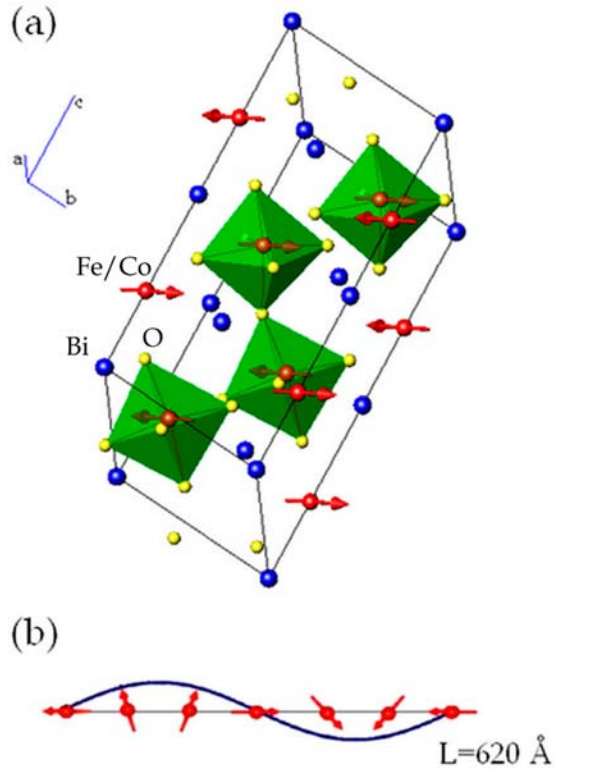

Figure 1. (After ref 9) (a) Schematic presentation of the $BiFeO_3$ unit cell in the hexagonal setting of space group $R3c$. The Bi, Fe/Co, and O ions are shown with blue, red, and yellow symbols, respectively. The distorted FeO_6 octahedra are shown in green. The (almost) antiparallel Fe^{3+} magnetic moments are shown with red arrows. The lower part of the figure (b) shows that the magnetic moments' direction changes in a periodic way while the magnetic moment values are constant across the spiral length.[12]

For the undoped $BiFeO_3$ structure, the bond length dispersion Δ_6 for the FeO_6 octahedron is calculated (see Table 2). For the ideal perovskite, the bond length dispersion Δ = 0. The values of Δ for $BiFeO_3$ increase between 10 K and RT, while for $BiFe_{0.8}Co_{0.2}O_3$, Δ remains constant within statistical error.

The temperature dependence of the lattice parameters (hexagonal setting of $R3c$) of $BiFe_{0.8}Co_{0.2}O_3$ is shown in Figure 2. The numerical values are given in the SI. One can see a positive thermal expansion similar to that observed for $BiFeO_3$.[39]

The magnetic contributions to the neutron powder diffraction patterns of $BiFe_{0.8}Co_{0.2}O_3$ and $BiFeO_3$ for the d region when the only magnetic scattering contributes to the diffraction maxima are presented as a function of temperature and are shown in Figure 3. Despite similarities in the crystal structures, the magnetic ordering in $BiFe_{0.8}Co_{0.2}O_3$ is not the same as in $BiFeO_3$.

At 10 K, $BiFe_{0.8}Co_{0.2}O_3$ shows magnetic satellite Bragg peaks similar to those observed in $BiFeO_3$,[12,34] indicating SMSS magnetic ordering. In a neutron diffraction pattern, the SMSS ordering gives four magnetic satellite reflections in the neutron powder diffraction pattern as explained in ref 12 (see also description in the SI). The SMSS structure is described with a modulation vector $\mathbf{q} = \delta\mathbf{a}^* + \delta\mathbf{b}^*$, where $\delta \approx 0.0045$[12,34] in the

dx.doi.org/10.1021/ic402427q | Inorg. Chem. 2013, 52, 13269−13277

Table 2. Selected Interatomic Distances (in Å) and Bond Angles (in deg) and Displacement Parameters *t* and *s*, Determined for the Pure $BiFeO_3$ (Column 1) and the Co-Doped $BiFe_{0.8}Co_{0.2}O_3$ (Column 2) Compounds at *T* = 10 K Compared with Those Obtained at *T* = 295 K in Columns 3 and 4, Respectively[a]

	1	2	3	4
	$BiFeO_3$ (x = 0) T = 10 K	BFCO (x = 0.20) T = 10 K	$BiFeO_3$ (x = 0) T = 295 K	BFCO (x = 0.20) T = 295 K
Fe/Co−O (×3)	1.9507(10)	1.9359(12)	1.9470(10)	1.9405(12)
Fe/Co−O (×3)	2.1047(10)	2.0860(11)	2.1142(10)	2.0930(13)
Δ_6	0.00144	0.00139	0.00169	0.00143
s [Bi displ.]	0.04839(5)	0.04500(6)	0.04828(6)	0.04500(6)
t [Fe displ.]	0.01885(6)	0.01790(7)	0.01905(7)	0.01800(7)
Bi−Fe/Co (×1)	3.0501(5)	3.0585(7)	3.0625(6)	3.0711(7)
Bi−Fe/Co (×3)	3.3018(6)	3.2916(9)	3.3077(5)	3.2998(6)
Bi−Fe/Co (×3)	3.5758(6)	3.5400(8)	3.5800(6)	3.5487(8)
Bi−Fe/Co (×1)	3.8675(5)	3.8007(8)	3.8735(5)	3.8139(8)
Bi−O (×3)	2.2603(9)	2.2818(13)	2.2693(10)	2.2890(12)
Bi−O (×3)	2.5240(8)	2.5093(14)	2.5314(8)	2.5153(11)
Bi−O (×3)	3.2117(9)	3.1731(13)	3.2117(9)	3.1806(10)
Bi−O (×3)	3.4441(9)	3.3726(12)	3.4477(10)	3.3841(11)
Fe/Co−O−Fe/Co	154.79(16)	155.80(18)	155.02(18)	155.77(21)
O−Fe/Co−O	164.97(19)	165.80(22)	165.02(21)	165.75(24)

[a]The Fe−O distances are inside the FeO_6 octahedra. For the doped compound, the Fe and Co ions occupy the same Wyckoff positions. The Fe/Co−O bond length dispersion parameter Δ_6 is calculated with eq 1. The displacement parameters, *t* and *s*, are calculated by using eqs 2 and 3, respectively.

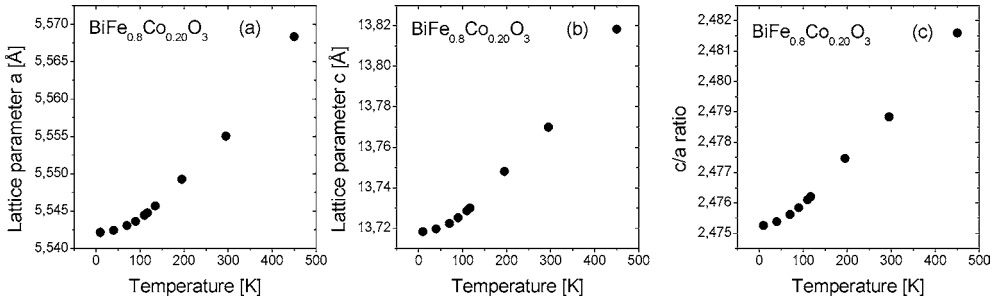

Figure 2. Temperature dependence of the unit cell parameters *a* and *c* and their ratio *c*/*a* determined for $BiFe_{0.8}Co_{0.2}O_3$ given in the hexagonal setting of the space group *R*3*c*.

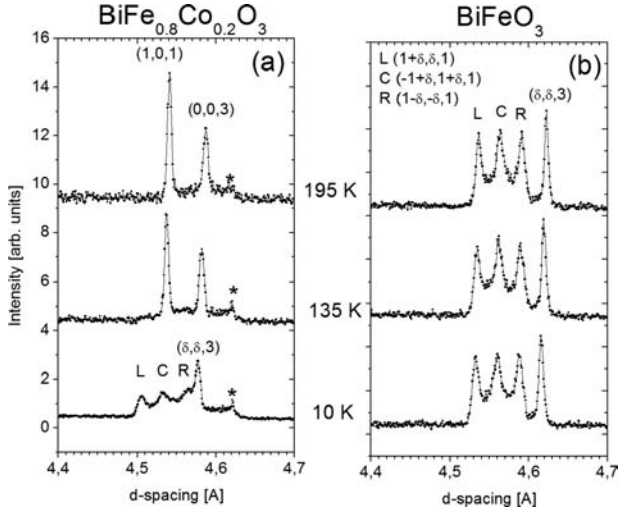

Figure 3. Neutron diffraction patterns for $BiFe_{0.8}Co_{0.2}O_3$ (left panel) and the parent $BiFeO_3$ compound (right panel)[34] for three temperatures: 10, 135, and 195 K. The solid symbols are experimental data. The indexing of the purely magnetic peaks is shown above each pattern (see SI). The stars indicate an instrumental artifact.

hexagonal setting of the space group *R*3*c*. At 10 K, we obtain a value of δ = 0.0044(2) for $BiFe_{0.8}Co_{0.2}O_3$, i.e., a similar value to that reported for $BiFeO_3$ at 10 K, δ = 0.0046(1).[34] Taking into account the lattice parameter *a* (see Table 1) at *T* = 10 K, the SMSS modulation lengths, $\lambda_M = a/(2\delta)$, are 630 and 605 Å for $BiFe_{0.8}Co_{0.2}O_3$ and $BiFeO_3$, respectively. The magnetic satellites observed for $BiFe_{0.8}Co_{0.2}O_3$ are broader than those of $BiFeO_3$. This effect can be due to a smaller magnetic domain size in $BiFe_{0.8}Co_{0.2}O_3$. The microstrains and possible grain size distributions present in the sample may also contribute to this effect. A complicated line shape and insufficient statistical accuracy of the data do not permit us to describe analytically these effects.

The neutron powder diffraction patterns for $BiFe_{0.8}Co_{0.2}O_3$ show a transition between SMSS ordering below 100 K and an antiferromagnetic G-type[40] ordering above 120 K (see Figure 3a). The neutron diffraction patterns observed at 135 and 195 K show (only) two maxima, (1,0,1) and (0,0,3), which are characteristic for a collinear G-type antiferromagnetic (G-AFM) ordering.[40] The Fe/Co magnetic moment direction (shown in Figure 3a) was determined using the intensity ratio of these maxima. It was found that the magnetic moments are perpendicular to the hexagonal *c*-axis. The angle between the magnetic moment direction and the *c*-axis is determined as 90

dx.doi.org/10.1021/ic402427q | Inorg. Chem. 2013, 52, 13269−13277

± 10°. The magnetic phase transition between the SMSS modulated structure and G-AFM observed in $BiFe_{0.8}Co_{0.2}O_3$ was not observed in the parent $BiFeO_3$ compound (see Figure 3b), preserving the SMSS structure up to the Néel temperature.[15,16]

The change of the spin structure from SMSS to G-AFM leads to the enhancement of the ferromagnetic moment, as shown by the magnetization curves for $BiFeO_3$ and $BiFe_{0.8}Co_{0.2}O_3$ presented in Figure 4.

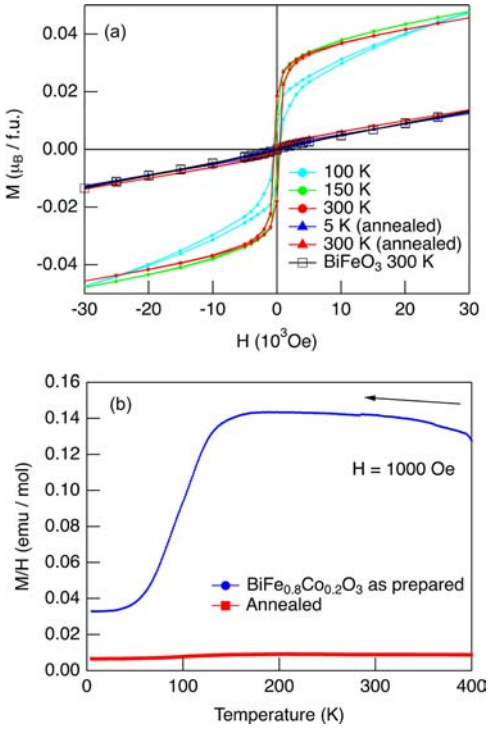

Figure 4. (a) Magnetization curve for $BiFeO_3$, as-prepared $BiFe_{0.8}Co_{0.2}O_3$, and $BiFe_{0.8}Co_{0.2}O_3$ after heat treatment at 873 K measured at various temperatures. (b) Temperature dependence of the magnetic susceptibility of as-prepared $BiFe_{0.8}Co_{0.2}O_3$ and $BiFe_{0.8}Co_{0.2}O_3$ after annealing at 573 K, measured in a magnetic field of 1000 Oe on cooling.

One can notice that at T = 5 K the ferromagnetic moment was negligible for $BiFe_{0.8}Co_{0.2}O_3$, just like in pure $BiFeO_3$. On the other hand, saturation magnetization of 0.03 μ_B/f.u. was observed at 300 K. It is clear from the temperature dependence of the susceptibility, shown in Figure 4b, that the magnetic transition appears at around 120 K, i.e., at a temperature where the phase transition from the cycloidal (SMSS) phase to the G-type antiferromagnetic phase is observed in the neutron diffraction data (see, for example, Figure 3).

Unfortunately, from our present neutron diffraction data analysis it is not possible to detect the existence of a ferromagnetic contribution of about 0.03 μ_B/f.u., which is observed in magnetization results and was detected in SANS studies.[14] The values of the ordered magnetic moment per one Fe/Co position refined from neutron diffraction data are shown in Figure 5. The numerical values are given in the SI (see Table S2). The ordered magnetic moment per one Fe/Co position is similar for both magnetic structures of $BiFe_{0.8}Co_{0.2}O_3$, i.e., SMSS and G-AFM. The phase transition from SMSS to G-AFM structure in $BiFe_{0.8}Co_{0.2}O_3$ on heating between 100 and 120 K may be interpreted as a sign of the spin bunching process

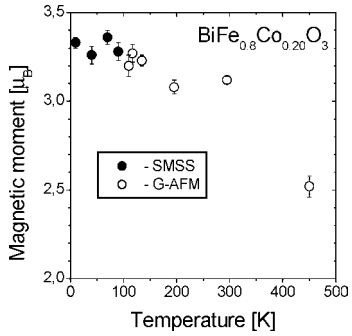

Figure 5. Temperature dependence of the ordered magnetic moment at shared Fe/Co positions in $BiFe_{0.8}Co_{0.2}O_3$ determined for the SMSS structure (solid symbols) and G-type antiferromagnetic ordering (open symbols) by using neutron diffraction.

described earlier for the magnetic cycloid.[41] The G-AFM ordering exists in $BiFe_{0.8}Co_{0.2}O_3$ at T = 453 K.

3B. Neutron Diffraction Studies of $BiFe_{0.8}Co_{0.2}O_3$ at 573 K. When heated above RT, a new monoclinic phase of $BiFe_{0.8}Co_{0.2}O_3$ described with the space group *Cm* appears. This phase is similar to the tetragonal structure of $BiCoO_3$[42] and to the recently reported monoclinic structure of $BiFe_{0.7}Co_{0.3}O_3$.[29] In this monoclinic structure, the Fe/Co ions are coordinated by five oxygen ions in a pyramidal configuration. This is different from the six oxygen ions in the octahedral coordination, which occurs in the rhombohedral *R*3*c* structure (see Figure 7). The $BiFe_{0.8}Co_{0.2}O_3$ sample shows

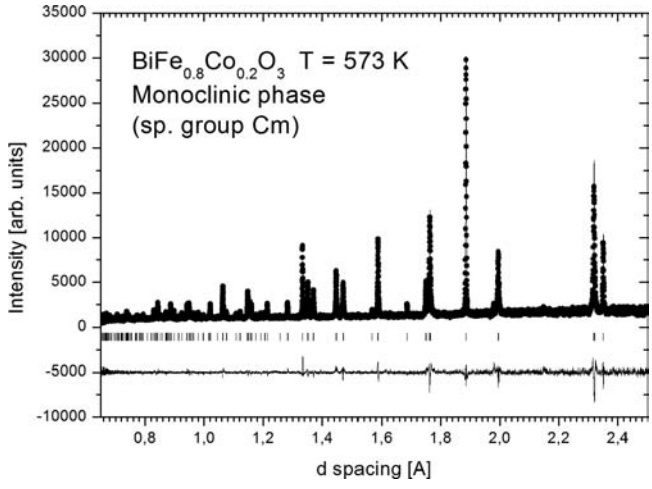

Figure 6. Results of the Rietveld refinement of the TOF neutron diffraction pattern of $BiFe_{0.8}Co_{0.2}O_3$ at 573 K. The experimental data are shown with solid symbols, the calculated pattern is shown with a continuous line, and the difference curve is shown below. The ticks with the expected Bragg peak positions for the monoclinic crystal structure (space group *Cm*) are shown below.

a single phase monoclinic *Cm* structure at 573 K (see Figure 6). The structural parameters obtained by using the Fullprof program at 573 K are given in Tables 3 and 4.

The neutron diffraction pattern of $BiFe_{0.8}Co_{0.2}O_3$ at 573 K does not show any sign of long-range magnetic ordering. The atomic displacement factor for Bi is considerably larger than for other ions. This effect is similar to that observed in the rhombohedral *R*3*c* phase (see Table 1).

The pyramidal FeO_5 polyhedron shows one short Fe−O bond (~1.83 Å) along the pyramid axis. Four O^{2-} neighbors

dx.doi.org/10.1021/ic402427q | Inorg. Chem. 2013, 52, 13269−13277

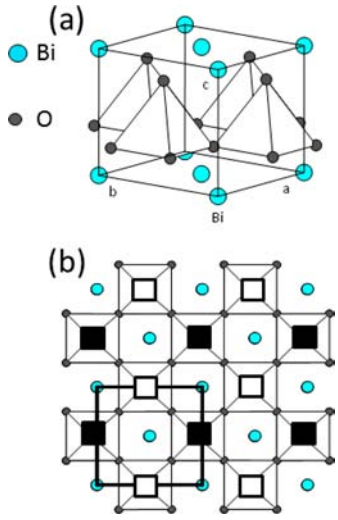

Figure 7. (a) Schematic presentation of the monoclinic unit cell of $BiFe_{0.8}Co_{0.2}O_3$ (space group *Cm*, $Z = 2$). The Fe/Co positions have pyramidal coordinated oxygen neighbors. (b) Schematic view of the C-AFM ordering in the $BiFe_{0.8}Co_{0.2}O_3$ lattice seen along the monoclinic *c*-axis. The square drawn with thick lines in the bottom-left corner shows the monoclinic unit cell. The black/white squares represent the up/down orientation of the antiferromagnetically ordered magnetic moments of Fe/Co atoms located in each pyramid (see Section 3C).

Table 3. Structural Parameters of $BiFe_{0.8}Co_{0.2}O_3$at 573 K As Determined by Neutron Diffraction[a]

atom	site	*x*	*y*	*z*	*B* [Å^2]	occup.
Bi	2a	0	0	0	2.00(4)	1.0
Co	2a	0.5034(7)	0	0.4294(4)	0.90(3)	0.2
Fe	2a	0.5034(7)	0	0.4294(6)	0.90(3)	0.8
O	2a	0.5439(7)	0	0.8167(6)	1.37(3)	1.0
O	4b	0.2498(8)	0.2477(7)	0.2913(4)	1.37(3)	1.0

[a]The monoclinic crystal structure is described within the space group *Cm* with the lattice constants $a = 5.33416(7)$ Å, $b = 5.33424(7)$ Å, $c = 4.70269(3)$ Å, and $\beta = 90.0935(9)°$. There is no long-range magnetic ordering in $BiFe_{0.8}Co_{0.2}O_3$ at 573 K. The agreement factors are $R_p = 9.19$, $R_{wp} = 11.3$, $R_{exp} = 7.50$, $\chi^2 = 2.27$.

are located in the basal plane, forming a slightly distorted square with Fe−O bonds of ∼2.00 Å. The remaining sixth O^{2-} neighbor is located on the axis pyramid at a larger distance, ∼2.89 Å. The bond length dispersion parameters Δ_5 have been calculated for the pyramid according to eq 1 . If one considers also the sixth oxygen neighbor at ∼2.89 Å, the value of Δ_6 can also be calculated. The values of Δ_5 and Δ_6 both show that the Fe/Co−O neighborhood distortion increases with increasing Co content in the $BiFe_{1-x}Co_xO_3$ $x = 0.2$, 0.3, and 1.0 compounds. The same applies also to the dispersion of the Bi−Fe/Co and Bi−O distances.

The schematic presentation of the $BiFe_{0.8}Co_{0.2}O_3$ monoclinic *Cm* unit cell is given in Figure 7a. The antiferromagnetic C-type ordering of Fe/Co magnetic moments is shown in Figure 7b and is discussed in the next section.

3C. Neutron Diffraction Studies of Annealed $BiFe_{0.8}Co_{0.2}O_3$. While heating the $BiFe_{0.8}Co_{0.2}O_3$ sample to 573 K, neutron diffraction measurements were also performed at 453 K. At this transition temperature, a part of the sample shows relatively broad peaks indicative of a precursor of the monoclinic *Cm* phase. At the intermediate temperatures, a coexistence of rhombohedral *R3c* and monoclinic *Cm* phases

Table 4. Selected Interatomic Distances (in Å) and Bond Angles (in deg) and Bond Length Dispersion Parameters Δ_5 and Δ_6, Determined for $BiFe_{0.8}Co_{0.2}O_3$ (Monoclinic *Cm*) at $T = 573$ K Compared with Literature Data for $BiFe_{0.7}Co_{0.3}O_3$ (Monoclinic *Cm*) at RT[29] and $BiCoO_3$ (Tetragonal *P4mm*) at 520 K[42,a]

	BFCO ($x = 0.20$) 573 K this paper	BFCO ($x = 0.30$) 295 K[29]	$BiCoO_3$ 520 K[42]
Fe/Co−O1 (×1)	1.833(3)	1.808(8)	1.711(5)
Fe/Co−O2 (×2)	1.999(3)	1.933(8)	2.025(2)
Fe/Co−O2 (×2)	1.991(3)	2.032(8)	2.025(2)
Fe/Co−O1 (×1)	2.890(3)	2.904(8)	3.030(5)
Δ_5	0.00109	0.00181	0.00410
Δ_6	0.02743	0.02990	0.03744
Bi−Fe/Co (×1)	3.334(3)	3.204(8)	3.347(5)
Bi−Fe/Co (×2)	3.345(2)	3.327(8)	3.347(5)
Bi−Fe/Co (×1)	3.357(2)	3.449(8)	3.347(5)
Bi−Fe/Co (×1)	3.783(2)	3.605(8)	3.777(5)
Bi−Fe/Co (×2)	3.767(2)	3.794(9)	3.777(5)
Bi−Fe/Co (×1)	3.799(2)	3.977(9)	3.777(5)
Bi−O2 (×2)	2.322(5)	2.229(8)	2.266(5)
Bi−O2 (×2)	2.340(5)	2.417(8)	2.266(5)
Bi−O1 (×1)	2.580(5)	2.495(8)	2.824(6)
Bi−O1 (×2)	2.813(5)	2.815(8)	2.824(6)
Bi−O1 (×1)	3.028(5)	3.108(8)	2.824(6)
Bi−O2 (×2)	3.827(5)	3.752(8)	3.938(6)
Bi−O2 (×2)	3.832(5)	3.942(8)	3.938(6)
Fe/Co−O2−Fe/Co	141.95(0.82)	142.02(1.75)	135.19(1.40)
O2−Fe/Co−O2	141.95(0.85)	142.02(1.75)	135.19(1.40)
O1−Fe/Co−O2	113.67(0.87)	110.76(2.00)	112.40(1.32)
O1−Fe/Co−O2	104.33(0.88)	107.20(2.00)	112.40(1.32)

[a]The first three Fe−O distances listed correspond to the Fe/Co−O bonds located inside the Fe/CoO_5 pyramids. For the doped compound, the Fe and Co ions occupy the same Wyckoff positions. The Fe/Co−O bond length dispersion parameters Δ_5 and Δ_6 are calculated for the Fe/Co−O_5 pyramids and Fe/Co−O_6 octahedra by using eq 1.

was observed. This was confirmed later with laboratory X-ray diffraction as well; the as-prepared rhombohedral $BiFe_{0.8}Co_{0.2}O_3$ sample changed into a mixture of monoclinic and rhombohedral phases after annealing. The lattice constants of the *Cm* precursor phase at $T = 453$ K were determined. It was, however, not possible to reliably determine the positional and atomic displacement parameters of the *Cm* precursor phase at $T = 453$ K.

After annealing at 573 K, the $BiFe_{0.8}Co_{0.2}O_3$ sample (with structural details given in Tables 3,4) was cooled to RT and neutron diffraction was measured on this annealed sample. The coexistence of both the *R3c* and *Cm* phases is observed in the annealed sample at RT. It was not possible to determine the positional and atomic displacement parameters of both the *Cm* and *R3c* phases because of peak-shape changes due to the

dx.doi.org/10.1021/ic402427q | *Inorg. Chem.* 2013, 52, 13269−13277

Table 5. Lattice Parameters for the Monoclinic Phase (*Cm* Space Group) of $BiFe_{0.8}Co_{0.2}O_3$ Determined by Neutron Diffraction (HRPD) for Three Temperatures

temp [K]	*a* [Å]	*b* [Å]	*c* [Å]	*β* [deg]	vol [Å^3]
573	5.33416(7)	5.33424(7)	4.70269(3)	90.093(1)	133.8087(26)
453	5.32533(12)	5.32412(12)	4.70468(10)	90.896(2)	133.3741(51)
295[a]	5.32046 (5)	5.31129(5)	4.70875(4)	91.989(9)	132.9821(21)

[a]The result at 295K is obtained for the annealed sample.

Table 6. Lattice Constants and Ordered Magnetic Moments at RT of the Rhombohedral (*R3c*) Phase of $BiFe_{0.8}Co_{0.2}O_3$ Observed for As-Prepared $BiFe_{0.8}Co_{0.2}O_3$ Sample and for the Same Sample after Annealing at 573 K

sample	*a* [Å]	*c* [Å]	*c*/*a*	M_AFM	*R3c*:*Cm*
as-prepared	5.55507(1)	13.77001(4)	2.47882	3.120(22)	100:0
annealed	5.55524(2)	13.77060(29)	2.47885	3.208(170)	32:68

microstructure introduced during the phase transformations. It was, however, possible to determine the lattice constant of both *R3c* and *Cm* phases in the annealed sample. The unit cell values determined for the *Cm* phase as a function of temperature are given in Table 5.

The temperature changes of monoclinic structural parameters observed for $BiFe_{0.8}Co_{0.2}O_3$ agree with those reported for $BiFe_{0.7}Co_{0.3}O_3$:[29] the monoclinic angle *β* steeply increases with decreasing temperature, while the lattice constant *c* shows a negative thermal expansion. The *Cm* phase transforms partially to the rhombohedral *R3c* with decreasing temperature. The unit cell values for the *R3c* phase in the as-prepared and annealed $BiFe_{0.8}Co_{0.2}O_3$ samples are compared in Table 6. One can see that the annealing process leads to the formation of a rhombohedral *R3c* structure with unit cell parameters in close agreement (about 0.01% relative difference) with those of the as-prepared rhombohedral *R3c* phase.

Selected parts of neutron diffraction patterns of $BiFe_{0.8}Co_{0.2}O_3$ in the *Cm* phase are shown for two temperatures, 453 and 295 K (after annealing), in Figure 8a.

The *Cm* phase of $BiFe_{0.8}Co_{0.2}O_3$ has a C-AFM[42] antiferromagnetic ordering at RT, as shown with diffraction data in Figure 8b. A schematic plot of the monoclinic unit cell with the magnetic moments ordering is shown in Figure 7b. The splitting of the magnetic reflections due to the monoclinic symmetry gives information on the magnetic moment direction in the *Cm* phase of $BiFe_{0.8}Co_{0.2}O_3$. The experimental intensity ratio can be described by assuming C-AFM ordering with the Fe/Co magnetic moment $\mathbf{M} = [-2.14, 1.39, 0.68]\ \mu_B$ (the monoclinic setting, *Cm*). Therefore, the magnetic moment per one Fe/Co site at RT is equal to $M = 2.62\ \mu_B$. There is no long-range magnetic ordering in the monoclinic *Cm* phase of $BiFe_{0.8}Co_{0.2}O_3$ at $T = 453$ K, as shown in Figure 8b.

The *R3c* phase of the annealed $BiFe_{0.8}Co_{0.2}O_3$ remains unchanged after cooling to 40 K. It keeps the collinear G-AFM ordering and shows no trace of the SMSS ordering.

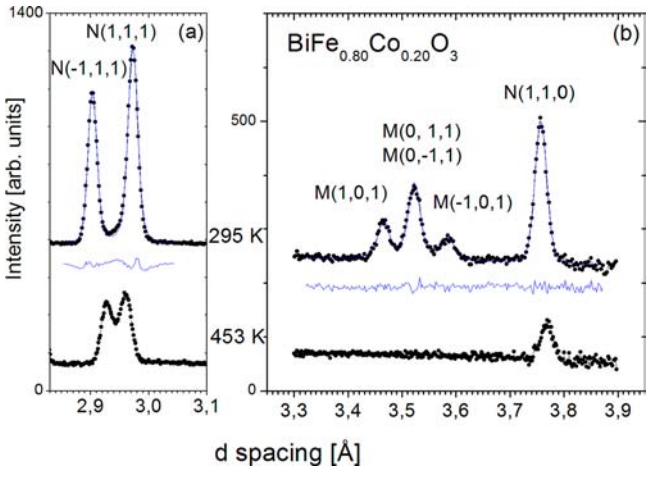

Figure 8. Selected parts of the TOF neutron powder diffraction patterns of $BiFe_{0.8}Co_{0.2}O_3$ at 453 and 295 K after heat treatment. (a) Nuclear reflections (1,1,1) and (−1,1,1) split due to the monoclinic structure (space group *Cm*). (b) Peaks due to the antiferromagnetic ordering present at 295 K and absent at 453 K. The nuclear and magnetic Bragg peaks in the *Cm* phase at 295 K were fitted. The results are shown as a continuous line, and the difference curve is shown below.

4. DISCUSSION

The crystal and magnetic structures of $BiFeO_3$ and $BiFe_{0.8}Co_{0.2}O_3$ as a function of temperature are summarized in Table 7.

The Co doping induces important changes in both the crystal structure and magnetic ordering of $BiFeO_3$. We can conclude also that Co substitution changes the properties of the material in a different way than with Mn substitution, where the SMSS length increases with the Mn content.[27] The observed ordered magnetic moment in the *R3c* phase permitted us to determine the spin states of Fe and Co ions in $BiFe_{0.8}Co_{0.2}O_3$. As it is known for pyramid coordination of Co^{3+} ions in $BiCoO_3$, Co^{3+} is in the high-spin (HS) state with the ordered moment of 2.93 μ_B.[42] The refined magnetic moment at RT per Fe/Co position is 3.12 μ_B. It is smaller than the magnetic moment of Fe^{3+} ions in $BiFeO_3$ at RT, i.e., $M = 4.00(4)\ \mu_B$.[38] On the other hand, it is larger than the Co^{3+} magnetic moment in pure $BiCoO_3$.

In the rhombohedral *R3c* structure, the Fe/Co ions have an octahedral coordination, and it was suggested that the Co ions are in the low-spin state (LS) with the ordered magnetic moment of 0.29 μ_B.[24] The total ordered magnetic moment for $BiFe_{0.8}Co_{0.2}O_3$ is calculated in Table 8 as "calculated model": $M = 0.8M_{Fe} - 0.2M_{Co}$ (LS) (antiparallel), which gives $M_{Fe/Co} = 3.41\ \mu_B$ (SMSS) and $M_{Fe/Co} = 3.14\ \mu_B$ (G-AFM). These values are in good agreement with the experimental values, which are 3.33 and 3.12 μ_B, respectively (see Table 8). Our present results indicate the antiparallel arrangement of the Co and Fe magnetic moments in $BiFe_{0.8}Co_{0.2}O_3$. Recent neutron diffraction studies of low Co doped $BiFe_{0.98}Co_{0.02}O_3$[25] suggest a parallel arrangement of Co and Fe magnetic moments. Due to the small Co content ($x = 0.02$), the influence on the ordered

dx.doi.org/10.1021/ic402427q | Inorg. Chem. 2013, 52, 13269−13277

Table 7. Summary of Crystal Structures and Magnetic Orderings Observed in $BiFeO_3$ and $BiFe_{0.8}Co_{0.2}O_3$[a]

	$BiFeO_3$		$BiFe_{0.8}Co_{0.2}O_3$			
T range [K]	crystal structure	magnetic structure	crystal structure	magnetic structure	T [K]	M/H [emu/mol]
10−90	*R3c*	SMSS	*R3c*	SMSS	10	0.032
90−120	*R3c*	SMSS	*R3c*	SMSS+G-AFM	90	0.083
120−300	*R3c*	SMSS	*R3c*	G-AFM	120	0.121
300−453	*R3c*	SMSS	*R3c*+*Cm*	G-AFM+C-AFM	300	0.140
573	*R3c*	SMSS	*Cm*	paramagnetic		

[a]*R3c* and *Cm* refer to the rhombohdral and monoclinic phases (see text). SMSS refers to space-modulated spin structure,[12,13] while G-AFM and C-AFM[42] refer to antiferromagnetic orderings.

Table 8. Ordered Magnetic Moments, *M*, for Fe/Co Position in the *R3c* Rhombohedral and *Cm* Phases of As-Prepared and Annelaed $BiFe_{0.8}Co_{0.2}O_3$ Sample Determined Using Neutron Diffraction[a]

			$BiFeO_3$ M [μ_B]	$BiFe_{0.8}Co_{0.2}O_3$ M [μ_B]	
space group	magnetic ordering	T [K]	from ref 38	exptl (present paper)	calcd (model)
R3c	SMSS	10	4.34	3.33	3.41
R3c	G-AFM	295	4.00	3.12	3.14
Cm	C-AFM	295	4.00[b]	2.62	2.61

[a]Experimental results are compared with the Fe/Co magnetic moment value calculated assuming opposite directions of magnetic moments of Fe and Co(LS/HS) in the SMSS, G-AFM, and C-AFM magnetic structures. [b]Taken the same as for *R3c*.

magnetic moment is comparable with the statistical error,[25] and the question of parallel or antiparallel arrangement has no clear answer. In the present study with (x = 0.20), the antiparallel arrangement explains the experimental results (see Table 8).

In the monoclinic *Cm* structure, the same antiparallel arrangement of Fe and Co magnetic moments explains the results. The Fe/Co ions have a pyramidal coordination, and it is assumed that the Co ions are in the high-spin state with the ordered magnetic moment of 2.93 μ_B as in $BiCoO_3$.[42] In this model, for the monoclinic *Cm* phase the calculated value is $M_{Fe/Co} = 0.8M_{Fe} - 0.2M_{Co}(HS)$ (antiparallel) = 2.61 μ_B (C-AFM) at RT. This in agreement with the experimental value 2.62 μ_B, as shown in Table 8.

It is important to note that the SMSS magnetic ordering in the *R3c* phase after annealing is not recovered down to 40 K and the material shows G-AFM ordering. Therefore, Co substitution and subsequent annealing at 300 °C can be a method to suppress the SMSS ordering in $BiFe_{0.8}Co_{0.2}O_3$ also at low temperatures besides already known methods such as high magnetic fields and low dimensionality.

CONCLUSIONS

Our observation is that the structure of Co-doped $BiFeO_3$ differs from that of the Mn-doped $BiFeO_3$. We found a change from cycloidal to collinear antiferromagnetic ordering in $BiFe_{0.8}Co_{0.2}O_3$ below RT. This collinear magnetic ordering in $BiFe_{0.8}Co_{0.2}O_3$ coexists with weak ferromagnetism at RT. These findings may promote further theoretical studies and experimental searches for the expected linear ME effect in this substance.

ASSOCIATED CONTENT

Supporting Information

List of indices of magnetic satellite Bragg peaks. Figure showing the location of the magnetic satellites in reciprocal space. Table with the temperature dependence of the parameters of the crystal structure and magnetic ordering of $BiFe_{0.8}Co_{0.2}O_3$. This material is available free of charge via the Internet at http://pubs.acs.org.

AUTHOR INFORMATION

Corresponding Author

*E-mail: izabela@fuw.edu.pl.

Present Address

[#](W.-T. Chen) Center for Condensed Matter Sciences, National Taiwan University, No. 1, Sec. 4, Roosevelt Road, Taipei 10617, Taiwan.

Notes

The authors declare no competing financial interest.

ACKNOWLEDGMENTS

Thanks are due to A. Daoud-Aladine (ISIS) for help as the local contact in the neutron diffraction measurements. This research project has been supported by the European Commission under the Seventh Framework Programme through the Key Action: Strengthening the European Research Area, Research Infrastructures, Contract No. CP-CSA-INFRA-2008-1.1.1 and No. 226507-NMI3. Thanks are due to the Ministry of Science and Higher Education (Poland) and the Cabinet Office of the Government of Japan through its "Funding Program for Next Generation World-Leading Researchers" (GR032) for funding.

REFERENCES

(1) Smolenskii, G. A.; Chupis, I. E. *Soviet Physics−Uspekhi* **1982**, *25*, 175.
(2) Fiebig, M. J. *Phys. D: Appl. Phys.* **2005**, *38*, R123.
(3) Schmid, H. *Ferroelectrics* **1994**, *162*, 317.
(4) Khomskii, D. *Physics* **2009**, *2*, 20.
(5) Eerenstein, W.; Mathur, N. D.; Scott, J. F. *Nature* **2006**, *442*, 759.
(6) Fiebig, M.; Lottermoser, T.; Frőhlich, D.; Goltsev, A. V.; Pisarev, R. V. *Nature* **2002**, *419*, 818.
(7) Hur, N.; Park, S.; Sharma, P. A.; Ahn, J. S.; Guha, S.; Cheong, S.-W. *Nature* **2004**, *429*, 392.
(8) Kubel, F.; Schmid, H. *Acta Crystallogr. B* **1990**, *46*, 698.
(9) Palewicz, A.; Przeniosło, R.; Sosnowska, I.; Hewat, A. W. *Acta Phys. Pol.* **2010**, *117*, 296.
(10) Sosnowska, I.; Przeniosło, R.; Palewicz, A.; Wardecki, D.; Fitch, A. *J. Phys. Soc. Jpn.* **2012**, *81*, 044604.

(11) Wang, H.; Yang, C.; Lu, J.; Wu, M.; Su, J.; Li, K.; Zhang, J.; Li, G.; Jin, T.; Kamiyama, T.; Liao, F.; Lin, J.; Wu, Y. *Inorg. Chem.* **2013**, *52*, 2388.
(12) Sosnowska, I.; Peterlin-Neumaier, T.; Steichele, E. *J. Phys. C: Solid State Phys.* **1982**, *15*, 4835.
(13) Sosnowska, I.; Zvezdin, A. K. *J. Magn. Magn. Mater.* **1995**, *140*−*144*, 167.
(14) Ramazanoglu, M.; Laver, M.; Ratcliff, W.; Watson, S. M.; Chen, W. C.; Jackson, A.; Kothapalli, K.; Lee, S.; Cheong, S.-W.; Kiryukhin, V. *Phys. Rev. Lett.* **2011**, *107*, 207206.
(15) Sosnowska, I.; Loewenhaupt, M.; David, W. I. F.; Ibberson, R. M. *Phys. B* **1992**, *180*−*181*, 117.
(16) Delaire, O.; Stone, M. B.; Ma, J.; Huq, A.; Gout, D.; Brown, C.; Wang, K. F.; Ren, Z. F. *Phys. Rev. B* **2012**, *85*, 064405.
(17) Tabares-Muñoz, C.; Rivera, J. P.; Bezinge, A.; Monnier, A.; Schmid, H. *Jpn. J. Appl. Phys.* **1985**, *24*, 1051.
(18) Murashov, V. A.; Rakov, D. N.; Dubienko, I. S.; Zvezdin, A. K.; Ionov, W. M. *Sov. Phys. Cryst.* **1990**, *35*, 538.
(19) Wang, J.; Neaton, J. B.; Zheng, H.; Nagarajan, V.; Ogale, S. B.; Liu, B.; Viehland, D.; Vaithyanathan, V.; Schlom, D. G.; Waghmare, U. V.; Spaldin, N. A.; Rabe, K. M.; Wuttig, M.; Ramesh, R. *Science* **2003**, *299*, 1719.
(20) Park, T.-J.; Papaefthymiou, G. C.; Viescas, A. J.; Moodenbaugh, A. R.; Wong, S. S. *Nano Lett.* **2007**, *7*, 766.
(21) Petkov, V.; Selbach, S. M.; Einarsrud, M.-A.; Grande, T.; Shastri, S. D. *Phys. Rev. Lett.* **2010**, *105*, 185501.
(22) Xu, Q.; Zai, H.; Wu, D.; Qiu, T.; Xu, M. X. *App. Phys. Lett.* **2009**, *95*, 112510.
(23) Xu, Q.; Zhou, S.; Wu, D.; Uhlarz, M.; Tang, Y. K.; Potzger, K.; Xu, M. X.; Schmid, H. *J. Appl. Phys.* **2010**, *107*, 093920.
(24) Ray, J.; Biswal, A. K.; Acharya, S.; Ganesan, V.; Pradhan, D. K.; Vishwakarma, P. N. *J. Magn. Magn. Mater.* **2012**, *324*, 4084.
(25) Ray, J.; Biswal, A. K.; Acharya, Babu, P. D.; Siruguri, V.; Vishwakarma, P. N. *AIP Conf. Proc.* **2013**, *1512*, 1124.
(26) Sosnowska, I.; Loewenhaupt, M.; David, W. I. F.; Ibberson, R. M. *Mater. Sci. Forum* **1993**, *133*−*136*, 683.
(27) Sosnowska, I.; Schäfer, W.; Kockelman, W.; Anderson, K. H.; Troyanchuk, I. O. *Appl. Phys.* **2002**, *A74*, S1040.
(28) Azuma, M.; Niitaka, S.; Hayazkii, N.; Oka, K.; Takano, M.; Funakubo, H.; Shimakawa, Y. *Jpn. J. Appl. Phys.* **2008**, *47*, 7579.
(29) Oka, K.; Koyama, T.; Ozaaki, T.; Mori, S.; Shimakawa, Y.; Azuma, M. *Angew. Chem.* **2012**, *51*, 7977.
(30) Dieguez, O.; Iniguez, J. *Phys. Rev. Lett.* **2011**, *107*, 057601.
(31) Lu, H.-X.; Mao, X.-Y.; Wang, W.; Chen, X.-B. *Progress in Electromagnetics Research Symposium*; Hangzhou, China, March 24−28, 2008; The Electromagnetics Academy: Cambridge, MA.
(32) Wang, J.; Li, M.; Liu, X.; Liu, W.; Hu, Z.; Wang, S. *J. Porous Mater.* **2013**, *20*, 727.
(33) Luo, L.; Shen, K.; Xu, Q.; Zhou, Q.; Wei, W. *J. Alloys Compd.* **2013**, *558*, 73.
(34) Sosnowska, I.; Przeniosło, R. *Phys. Rev. B* **2011**, *84*, 144404.
(35) Ibberson, R. M.; David, W. I. F.; Knight K. S. *CLRC Report RAL-92-031*, 1992; Council for the Central Lab. of the Research Councils: Chilton, UK.
(36) Rodriguez-Carvajal, J. *Phys. B (Amsterdam, Neth.)* **1992**, *192*, 55.
(37) Megaw, H. D.; Darlington, C. N. W. *Acta Crystallogr. A* **1975**, *31*, 161.
(38) Fischer, P.; Połomska, M.; Sosnowska, I.; Szymański, M. *J. Phys. C: Solid State Phys.* **1980**, *13*, 1931.
(39) Palewicz, A.; Szumiata, T.; Przeniosło, R.; Sosnowska, I.; Margiolaki, I. *Solid State Commun.* **2006**, *140*, 359.
(40) Bertaut, E. F.; Forrat, F. *J. Phys. Radium* **1956**, *17*, 129. Bertaut, E. F. In *Magnetism III*; Rado, G. T.; Suhl, H., Eds.; Academic Press: New York, 1963; p 149.
(41) Solovyev, I. V. *Phys. Rev. B* **2012**, *85*, 05442.
(42) Belik, A. A.; Iikubo, S.; Kodama, K.; Igawa, N.; Shamoto, S.; Niitaka, S.; Azuma, M.; Shimakawa, Y.; Takano, M.; Izumi, F.; Takayama-Muromachi, E. *Chem. Mater.* **2006**, *18*, 798.

NOTE ADDED AFTER ASAP PUBLICATION

Tables 1, 2, 4, and 8 contained errors in the version published ASAP on November 1, 2013; the correct version reposted November 5, 2013.